2018 AIAA Aerospace Sciences Meeting
8–12 January 2018, Kissimmee, Florida

DOI: 10.2514/6.2018-0818
AIAA 2018-0818

Determination of the Critical Reynolds Number for Flow over Symmetric NACA Airfoils

Kianoosh Yousefi[1]
Department of Mechanical Enginering, University of Delaware, Newark, DE 19716 USA

and

Alireza Razeghi[2]
Department of Mechanical Engineering, Özyeğin University, Istanbul, 34794, Turkey

The determination of the critical Reynolds number is of practical importance in many engineering applications, particularly in determining the aerodynamic characteristics of air vehicles. In this study, we numerically investigated the laminar-turbulent transition location over NACA 0012, 0015, and 0018 airfoil profiles in order to determine their lower critical Reynolds number. To this end, a CFD FORTRAN code was developed based on the hybrid viscous-inviscid interaction method with an incorporated e^N transition method to model the boundary layer flow around airfoil profiles. The results, in general, indicated that the laminar-turbulent transition location over an airfoil is strongly dependent on the Reynolds number and moves toward the downstream as the Reynolds number decreases. The lower critical Reynolds number was then defined as the velocity at which the flow becomes laminar over the airfoil, which corresponds to the conditions that the transition point located at the trailing edge of the airfoil. The lower critical Reynolds number for flow over NACA 0012, 0015, and 0018 airfoils were, therefore, determined to be 1×10^5, 5×10^4, and 3.5×10^4, respectively. Moreover, the variations of the transition location with the angle of the attack showed that the transition point moves toward the leading edge of the airfoil as the angle of attack increases.

Nomenclature

C_D	=	Drag coefficient
C_L	=	Lift coefficient
Re_c	=	Chord Reynolds number, $\rho u_\infty c/\mu$
Re_{cr}	=	Critical Reynolds number, $\rho u_\infty x_{tr}/\mu$
Re_θ	=	Reynolds number based on the boundary layer momentum thickness, $\rho u_e \theta/\mu$
u_∞	=	Freestream velocity
u_e	=	Spatial velocity at the boundary layer edge
x_{tr}	=	Transition point
α_i	=	Spatial growth rate of the TS wav
δ^*	=	Boundary layer displacement thickness
θ_∞	=	Momentum thickness of the wake at downstream infinity
H	=	Boundary layer shape factor, δ^*/θ
N	=	Critical factor in the transition model
c	=	Chord Length
α	=	Angle of attack
δ	=	Boundary layer thickness
θ	=	Momentum thickness
μ	=	Viscosity
ρ	=	Density
ω	=	Frequency

[1] Research Assistant, Department of Mechanical Engineering, 126 Spencer Lab, Newark, DE 19716 USA.
[2] Ph.D. Student, Department of Mechanical Engineering, Özyeğin University, Istanbul, 34794, Turkey.

I. Introduction

The transition from laminar to turbulent flow considerably influences the mixing, drag, and pressure, and hence, the aerodynamic characteristics of air vehicles. The flow transition is primarily affected by the surface geometry, surface roughness, and upstream velocity, among other factors, and is best characterized by the critical Reynolds number[1]. The laminar flow over a smooth flat plate begins to transit to the turbulent flow at a Reynolds number of about 1×10^5 but does not become fully turbulent before the Reynolds number reaches much higher values, typically around 3×10^6. The Reynolds number of 5×10^5 is well established as the critical Reynolds number for flows over smooth flat plates. In practice, however, the critical Reynolds number may vary from nearly 1×10^5 to 3×10^6 for flows above a flat plate, depending on the surface roughness, turbulence level, and pressure variations along the surface[1-2]. The critical Reynolds number, in general, decreases by varying the thickness of body from a flat plate to a blunt body. The transition Reynolds number for flow across a circular cylinder or sphere is therefore about 2×10^5, and for most airfoil profiles is approximately within the range of 1×10^3 - 2×10^5, which strongly depends on the maximum thickness of an airfoil profile[3].

The aerodynamic performance of airfoils and streamlined bodies, in general, are a strong function of the laminar-turbulent transition, and consequently, the critical Reynolds number[1, 4]. However, the number of studies in the literature that investigated the critical Reynolds number or the transition Reynolds number over airfoil-shaped bodies, e.g. wings and blades, is limited mainly due to the variety of affecting parameters and the complexity of the transition. The studies of low-Reynolds-number airfoils[3, 5] have indicated that the boundary layer flow remains laminar for the Reynolds number between 1×10^3 and 1×10^4, and it is challenging to cause the flow to transit into a turbulent flow. The range of the Reynold number varying from 3×10^4 to 7×10^4 is of a great interest to micro air vehicle (MAV) designers as well as model aircraft builders. The choice of an airfoil profile in this regime is of significant importance since relatively thick airfoils, i.e. 6% and above, can produce considerable hysteresis effects caused by laminar separation with a subsequent transition to the turbulent flow. At Reynolds numbers above 7×10^4 and below 2×10^5, extensive laminar flow can be achieved, and therefore, airfoil performance improves, but the laminar separation bubble may still cause a problem for particular airfoils. For Reynolds Numbers greater than 2×10^5, the airfoil performance improves significantly, and for the overwhelming majority of airfoils, the regime is turbulent.

The transition of the laminar boundary layer to the turbulent boundary layer occurs when the chord Reynolds number is greater than the critical Reynolds number. Kraemer[6] studied three specific Göttinger airfoils including GÖ 801, GÖ 803, and GÖ 804, and demonstrated that the critical Reynolds number for average angles of attack is only slightly dependent on the angle of attack in the steady flow. Their results showed that the smallest value for the critical Reynolds number, i.e. the lower critical Reynolds number, is 6.2×10^4 and 5.5×10^4 for GÖ 801 and GÖ 803 airfoils, respectively. The critical Reynolds number of the GÖ 804 profile, which could not be determined through the experimental measurements, is much smaller than roughly 1×10^4. Mueller[7] conducted an experimental investigation on the relative location of the laminar separation and transition over Lissaman 7769 and Miley M06-13-128 airfoil sections at relatively low chord Reynolds numbers. It was observed that the increase of the Reynolds number or free-stream disturbance level resulted in earlier transition and reattachment of the free shear layer for both profiles. Brendel and Mueller[8] also studied the characteristics of the transitional separation bubbles that are generated on the Wortmann FX63-137 airfoil through velocity point measurements at different chord Reynolds numbers of 1×10^5, 1.5×10^5, and 2×10^5. The results indicated that the transitional Reynolds number, which ranged between 1.35×10^4 and 5.6×10^4, increases with increasing the Reynolds number at the separation point. The e^N method has been widely employed in numerical studies to predict the transition location over the past few decades[9-12]. Lian and Shyy[12] performed a computational study to determine the transition location over the SD7003 airfoil through coupling the momentum equations with the e^N transition method and employing a two-equation closure model for the Reynolds-averaged Navier–Stokes equations. It was shown that the transition position moves toward the leading edge (trailing edge) when the chord Reynold number increases (decreases).

The transition plays an integral role in determining the aerodynamic performance of airfoils, particularly low-Reynolds-number airfoils. The laminar and/or turbulent properties of the flow have a significant influence on the skin friction (transition) and separation, and therefore, on the lift and drag properties. In addition to the recent computational studies[13-15], many experimental investigations have been conducted to study the laminar-turbulent transition over the airfoils by using single-point flow measurement techniques, such as hot-wire anemometry[16-17], laser doppler velocimetry[18-19], and particle image velocimetry[20-22]. Compared to the literature on the transitional behavior of airfoils, there are relatively few studies focusing on determining the critical Reynolds number of airfoil profiles. In the current study, therefore, we numerically investigated the critical Reynolds number for flow over symmetrical NACA airfoils. The laminar-turbulent transition location over NACA 0012, NACA 0015, and NACA 0018 airfoil profiles are investigated to determine the critical Reynolds number at an angle of attack of zero degrees.

II. Computational Methods

To facilitate the present study, a FORTRAN code has been developed based on the hybrid viscous-inviscid interaction method[23-24] to predict the boundary layer flow around low-Reynolds-number airfoil profiles. The potential flow equations were considered for describing the inviscid, irrotational flow outside the boundary layer where a two-dimensional linear-vorticity panel method was employed for calculating the inviscid free-stream in direct- and inverse-modes. A two-equation integral formulation, i.e. integral momentum and kinetic energy shape parameter equations, was also used based on the dissipation closure for both laminar and turbulent flows to represent the viscous boundary layer. The viscous formulation in the streamwise direction can be expressed as,

$$\frac{d\theta}{d\xi} + (2 + H - M_e^2)\frac{\theta}{u_e}\frac{du_e}{d\xi} = \frac{C_f}{2} \tag{1}$$

$$\theta\frac{dH^*}{d\xi} + [2H^{**} + H^*(1 - H)]\frac{\theta}{u_e}\frac{du_e}{d\xi} = 2C_d - H^*\frac{C_f}{2} \tag{2}$$

where θ is the momentum thickness, ξ is the streamwise coordinate, $H = \delta^*/\theta$ is the shape factor, δ^* is the displacement thickness, M_e is the boundary-layer edge Mach number, u_e is the boundary-layer edge velocity, C_f is the skin-friction coefficient, $H^* = \theta^*/\theta$ is the kinetic energy shape factor, θ^* is the kinetic energy thickness, $H^{**} = \delta^{**}/\theta$ is the density shape factor, δ^{**} is the density thickness, and C_d is the dissipation coefficient. A rate equation for the shear stress coefficient was also considered to estimate the deviations of the turbulent boundary layer from the local equilibrium, which was replaced by the spatial amplification rate equation of the most-amplified Tollmien-Schlichting wave in the laminar regions. Both laminar and turbulent flows were treated with an e^N transition model and the discrete boundary layer equations were simultaneously resolved with the transition equations through a full Newton method. The details of inviscid and viscous formulations can be found in the references from Drela[23] and Drela and Giles[24]. The drag coefficient was obtained from the momentum conservation in the ξ-direction, which can be expressed in a dimensionless form as[25-26],

$$C_D = \frac{2\theta}{c} \tag{3}$$

where θ is the momentum thickness of the wake at the downstream infinity location and c is the airfoil chord length. The momentum thickness can be calculated as,

$$\theta = \int_0^{\delta} \frac{u}{u_e}\left(1 - \frac{u}{u_e}\right) d\zeta \tag{4}$$

where ζ is the transverse direction, and δ is the boundary layer thickness. It should be noticed here that the use of the boundary-layer edge velocity instead of the free-stream velocity in the momentum thickness calculations may cause drag underprediction, particularly for thick airfoils.

A. Transition Model

The e^N transition method is generally based on the linear stability analysis and Orr–Sommerfeld equation, which employs a spatial-amplification theory. The e^N method states that transition happens when the most unstable Tollmien–Schlichting wave in the boundary layer is grown by a factor of e^N, where N is defined as follows[12, 27],

$$N = max_{\omega}\tilde{n}(x_t, \omega) \tag{5}$$

$$\tilde{n}(x_t, \omega) = -\int_{x_0}^{x} \alpha_i(\omega)\ dx \tag{6}$$

where ω is the frequency, $\tilde{n}(x, \omega)$ is the amplitude growth of the disturbance along the chord of the airfoil with frequency ω, x_t is the transition position, x_0 is the onset location of instability, and $-\alpha_i$ is the spatial growth rate of the TS wave. For any velocity profile, the local disturbance growth rates can be concluded by solving the Orr–

Sommerfeld equation. The amplification factor is then calculated by integrating the growth rate. For incompressible flows, however, the amplification factor can be approximated by straight lines[12, 28] as,

$$\tilde{n} = \frac{d\tilde{n}}{dRe_\theta}(H)\left[Re_\theta - Re_{\theta_0}(H)\right] \tag{7}$$

where Re_θ is the Reynolds number based on the boundary layer momentum thickness defined as $Re_\theta = \rho u_e \theta/\mu$, Re_{θ_0} is the empirical critical Reynolds number, and H is the boundary layer shape factor defined as $H = \delta^*/\theta$ in which δ^* is the boundary-layer displacement thickness. For similar flows, the amplification factor can be determined by the following empirical expression,

$$\frac{d\tilde{n}}{dRe_\theta} = 0.01\{[2.4H - 3.7 + 2.5\tanh(1.5H - 4.65)]^2 + 0.25\}^{1/2} \tag{8}$$

For nonsimilar flows, however, Eq. (8) is not appropriate for determining the transition in separation bubbles. Thus, the amplification factor with respect to the streamwise coordinate can be written as,

$$\frac{d\tilde{n}}{d\xi} = \frac{d\tilde{n}}{dRe_\theta}\frac{1}{2}\left(\frac{\xi}{u_e}\frac{du_e}{d\xi} + 1\right)\frac{\rho_e u_e \theta^2}{u_e \xi}\frac{1}{\theta} \tag{9}$$

An explicit expression for the amplification factor then becomes,

$$\tilde{n}(\xi) = \int_{\xi_0}^{\xi} \frac{d\tilde{n}}{d\xi} d\xi \tag{10}$$

where ξ_0 is the point at which the momentum thickness Reynolds number equals the critical Reynolds number. The critical Reynolds number can be expressed by the following empirical expression[12, 24],

$$\log_{10} Re_{\theta_0} = \left(\frac{1.415}{H-1} - 0.489\right)\tanh\left(\frac{20}{H-1} - 12.9\right) + \frac{3.295}{H-1} + 0.44 \tag{11}$$

With this approach, the amplification factor is approximated with a relatively good accuracy. Furthur details can be found in the work of Lian and Shyy[12] and Drela and Giles[24]. It is also worth mentioning that the e^N approach assumes the following assumptions are satisfied; (1) the initial disturbance is infinitesimally small and (2) the laminar boundary layer is thin and gradually grows in the streamwise direction.

B. Grid Setup

The inviscid formulations were treated with the vortex panel method where a series of infinite, discrete bound vortices were placed on the airfoil profile, as shown in Fig. 1, in order to approximate a continuous distribution of vortices. In a two-dimensional flow field, the airfoil surface is divided into many piecewise straight line segments or so-called panels where the vortex sheets of strength γ are placed on each panel. These vortices that imitate the boundary layer around the airfoil are then risen to circulation, and consequently, lift. The number of panel nodes on the upper and lower side of the airfoil was examined to attain the node independence. The node-independence study is summarized in Table 1 and Table 2 and illustrated in Fig. 2 for the NACA 0012, NACA 0015, and NACA 0018 airfoils with a Reynolds number of 5×10^5 at angles of attack of 0 and 5 degrees. As a result, 180 panel nodes were selected for the current study.

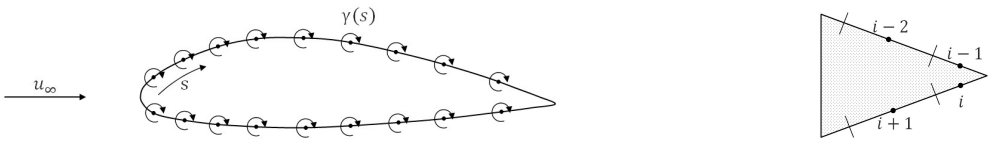

Figure 1. Sketch of the vortex panel method over an arbitrary, smooth airfoil along with the trailing edge details with vorticity distributions. A two-dimensional inviscid flow field over an airfoil generally consists of a free-stream flow, a vortex sheet of strength γ on the airfoil surface, and a source sheet of strength σ on the airfoil surface.

Table 1. Node independence study for NACA 0012, NACA 0015, and NACA 0018 airfoil profiles at a Reynolds number of 5×10^5 and an angle of attack of 0 degrees.

Number of Panel Nodes	NACA 0012		NACA 0015		NACA 0018	
	C_L	C_D	C_L	C_D	C_L	C_D
40	0.0	0.00606	0.0	0.00714	0.0	0.00798
80	0.0	0.00613	0.0	0.00723	0.0	0.00829
120	0.0	0.00615	0.0	0.00728	0.0	0.00838
140	0.0	0.00616	0.0	0.00730	0.0	0.00836
160	0.0	0.00617	0.0	0.00731	0.0	0.00841
170	0.0	0.00617	0.0	0.00730	0.0	0.00839
180	0.0	0.00617	0.0	0.00730	0.0	0.00838
200	0.0	0.00617	0.0	0.00730	0.0	0.00838

Table 2. Node independence study for NACA 0012, NACA 0015, and NACA 0018 airfoil profiles at a Reynolds number of 5×10^5 and an angle of attack of 5 degrees.

Number of Panel Nodes	NACA 0012		NACA 0015		NACA 0018	
	C_L	C_D	C_L	C_D	C_L	C_D
40	0.6251	0.01023	0.5553	0.00998	0.5307	0.01011
80	0.6273	0.01030	0.5572	0.01009	0.5253	0.01015
120	0.6274	0.01034	0.5532	0.01014	0.5228	0.01027
140	0.6274	0.01035	0.5524	0.01015	0.5217	0.01023
160	0.6274	0.01037	0.5495	0.01015	0.5217	0.01023
170	0.6274	0.01037	0.5481	0.01013	0.5212	0.01024
180	0.6274	0.01038	0.5490	0.01016	0.5215	0.01026
200	0.6274	0.01038	0.5490	0.01016	0.5215	0.01026

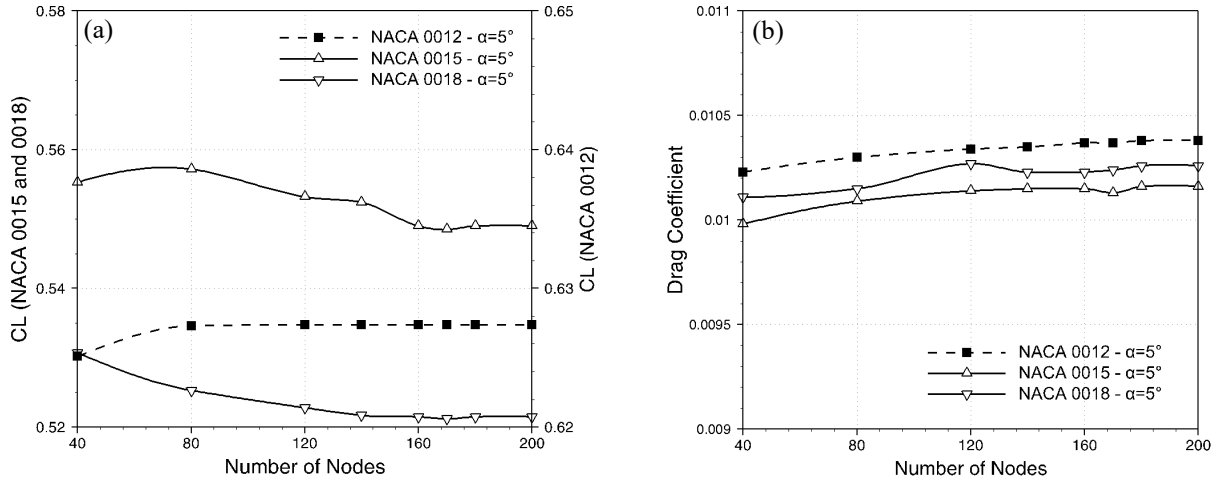

Figure 2. Node independence study for NACA 0012, NACA 0015, and NACA 0018 airfoil profiles at a Reynolds number of 5×10^5 and an angle of attack of 5 degrees for (a) lift coefficient and (b) drag coefficient.

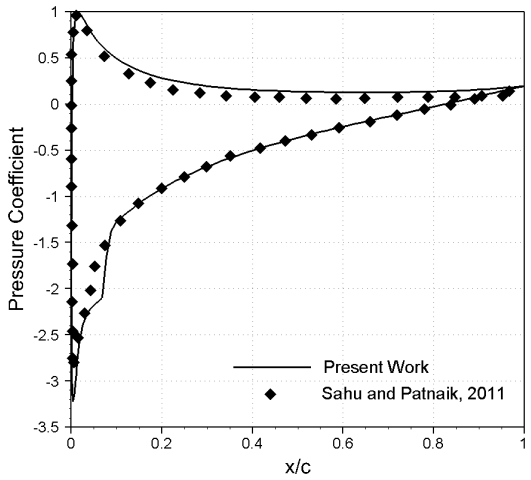

Figure 3. Pressure coefficient distribution over the NACA 0012 airfoil compared with the numerical results of Sahu and Patnaik[29] at a Reynolds number of 2.4 × 10^5 and an angle of attack 8°.

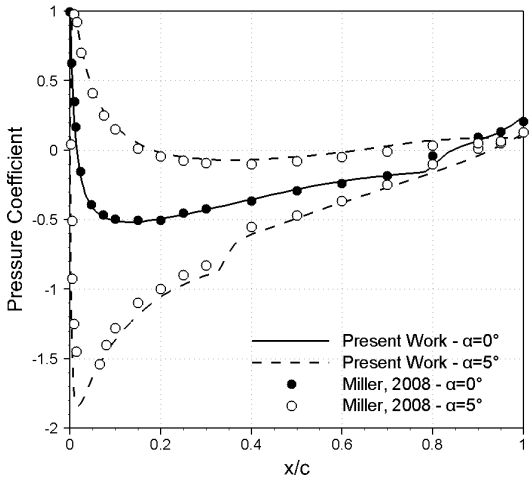

Figure 4. Pressure coefficient distribution over the NACA 0015 airfoil compared with the experimental measurements of Miller[30] at Reynolds number of 2.4 × 10^5 and angles of attack of 0° and 5°.

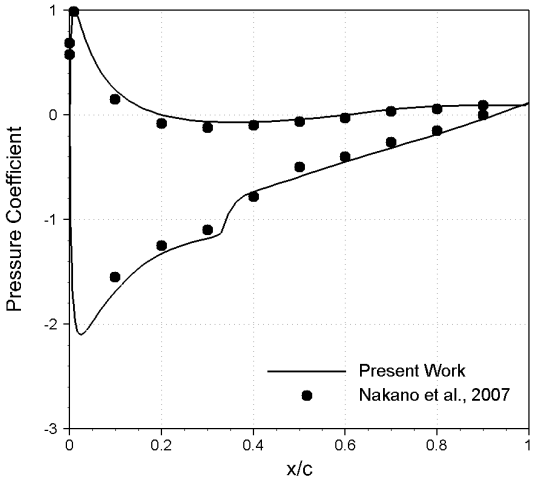

Figure 5. Pressure coefficient distribution over the NACA 0018 airfoil compared with the experimental results of Nakano et al.[31] at a Reynolds number of 1.6 × 10^5 and an angle of attack of 6°.

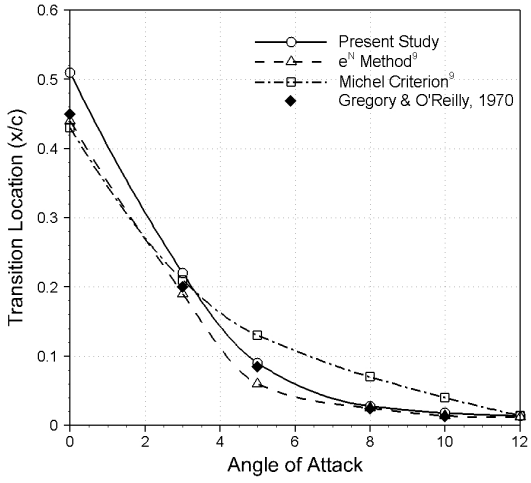

Figure 6. Comparison of transition locations between the current study and the experimental results of Gregory and O'Reilly[32] as well as the numerical results of Johansen and Sorensen[9] for the NACA 0012 airfoil at a Reynolds number of of 3 × 10^6.

C. Numerical Validation

The results of the current work including the pressure coefficient and transition location were compared with the existing numerical and experimental studies at different Reynolds numbers and angles of attack. The distribution of the pressure coefficient over NACA 0012, NACA 0015, and NACA 0018 airfoils is compared with the existing experimental and numerical results as demonstrated in Figs. 3, 4, and 5, respectively. The pressure coefficient of NACA 0012 airfoil is compared with the numerical results of Sahu and Patnaik[29] in Fig. 3 at a Reynolds number of 2.4 × 10^5 and an angle of attack of 8 degrees. Figure 4 presents a comparison between the pressure coefficient of the current work and the experimental measurements of Miller[30] for the NACA 0015 airfoil at a Reynolds number of 2.4 × 10^5 and angles of attack of 0 and 5 degrees. The pressure coefficient of NACA 0018 airfoil is also compared with the experimental work of Nakano et al.[31] in Fig. 5 when the Reynolds number was 1.6 × 10^5 and the angle of attack was 6 degrees. The transition location of the NACA 0012 airfoil was subsequently compared with the experimental measurements of Gregory and O'Reilly[32] and computational results of Johansen and Sorensen[9], as demonstrated in

Fig. 6, at a Reynolds number of 3×10^6 and different angles of attack varying from 0 to 5 degrees. The laminar-turbulent transition locations over the NACA 0015 airfoil were also compared with the laboratory measurements of Baek and Fuglsang[33] in Fig. 7 for the Reynolds numbers of 3×10^6 and 6×10^6. Figure 8 also illustrates the variations of the transition location with the angle of attack for the NACA 0018 airfoil where the results of the current work are compared with experimental[34] and numerical[35] studies for the Reynolds numbers of 7×10^5 and 1×10^6. It can be observed from Figs. 3 through 8 that the computational results of the current work are in a complete agreement with experimental measurements.

III. Results and Discussion

The Reynolds number is an important parameter in order to determine whether the flow is laminar or turbulent. The critical Reynolds number varies between the upper and lower critical Reynolds number values. The upper critical Reynolds number is defined as the velocity at which the laminar flow no longer exists over an airfoil, while the velocity at which the flow becomes laminar over an airfoil corresponds to the lower critical Reynolds number. The lower critical Reynolds number, therefore, can be achieved when the transition point is located at the trailing edge of the airfoil.

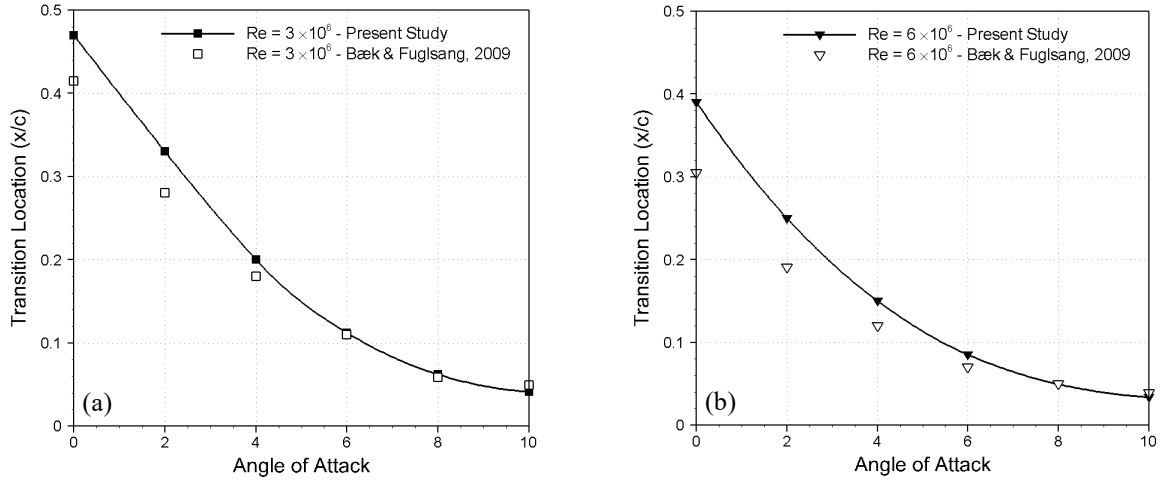

Figure 7. Comparison of transition locations between the current study and the experimental measurements of Bæk and Fuglsang[33] for the NACA 0015 airfoil at Reynolds numbers of (a) 3×10^6 and (b) 6×10^6.

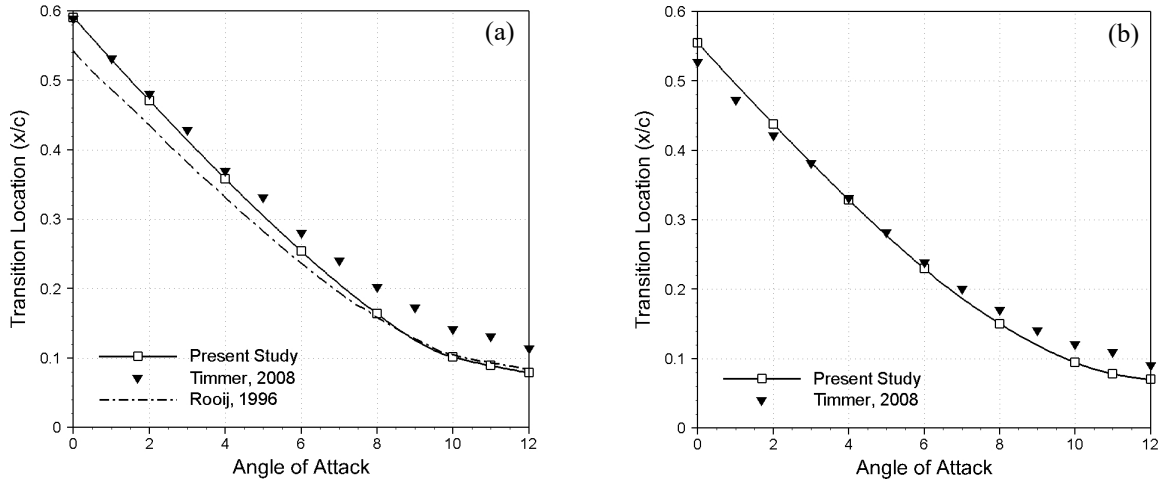

Figure 8. Comparison of transition locations between the current study and the experimental measurements of Timmer[34] as well as the numerical results of Rooij[35] for NACA 0018 airfoil at the Reynolds numbers of (a) 7×10^5 and (b) 1×10^6.

We determined, in the current study, the critical Reynolds number for flow over NACA 0012, NACA 0015, and NACA 0018 airfoil profiles by estimating the laminar-turbulent transition location. The variations of the transition point with the Reynolds number is shown in Fig. 9. It can be observed that the transition location over an airfoil is a strong function of the Reynolds number and moves toward the downstream as the Reynolds number decreases. The transition position over NACA 0012, NACA 0015, and NACA 0018 airfoils was located at 0.7923, 0.6952, and 0.6256, respectively, at the Reynolds number of 5×10^5. By decreasing the Reynolds number, the laminar-turbulent transition point moves downstream to the point that located at the trailing edge of the airfoil, i.e. $x_{tr}/c \cong 1$, and the flow becomes laminar over the airfoil, which is corresponding to the lower critical Reynolds number. Therefore, the lower critical Reynolds number for flow over NACA 0012, NACA 0015, and NACA 0018 airfoil profiles is 1×10^5, 5×10^4, and 3.5×10^4, respectively, at the angle of attack of zero degrees. The variations of the transition location with the chord Reynolds number is reported in detail in Table 3. The transition from laminar to turbulent flow is essentially continuous and consists of a number of developing steps. In general, the transition process can be explained in four steps. The small two-dimensional waves are first produced and linearly amplified. These two-dimensional waves are then developed into finite three-dimensional waves and nonlinearly amplified. This leads to forming a turbulence spot in the flow, and finally, the turbulence spot propagates and fills the entire region with turbulence. Furthermore, Fig. 9 demostrates that the lower critical Reynolds number decreases with increasing the airfoil thickness from 1×10^5 for the NACA 0012 airfoil to 3.5×10^4 for the NACA 0018 airfoil, which is consistent with the literature[5,36-37].

The variations of the transition point with the angle of attack were also investigated which is demonstrated in Fig. 10 for the chord Reynolds numbers of 5×10^5 and 2×10^5. The transition point quickly moves upstream toward the leading edge of the airfoil as the angle of attack increases. This behavior is frequently reported in the literature[12, 38-40]. The transition location transferred from 0.7923, 0.6952, and, 0.6256 at an angle of attack of zero degrees to 0.0201, 0.0312, and 0.0511 at an angle of attack of 18 degrees for the NACA 0012, NACA 0015, and NACA 0018 airfoils, respectively, for the chord Reynolds number of 5 × 105. The transitional behavior over airfoil profiles is significantly important where several affecting parameters are involved. In the current study, therefore, we briefly considered the effects of the chord Reynolds number and the angle of attack on the laminar-turbulent transition location in addition to determining the critical Reynolds number.

IV. Conclusion

In the current paper, the lower critical Reynolds number for flow over NACA 0012, NACA 0015, and NACA 0018 airfoils is investigated by examining the laminar-turbulent transition over airfoils at an angle of attack of zero degrees. A CFD FORTRAN code was developed based on the hybrid viscous-inviscid interaction method with an incorporated e^N transition model in order to model the boundary layer flow around airfoil profiles. The potential flow

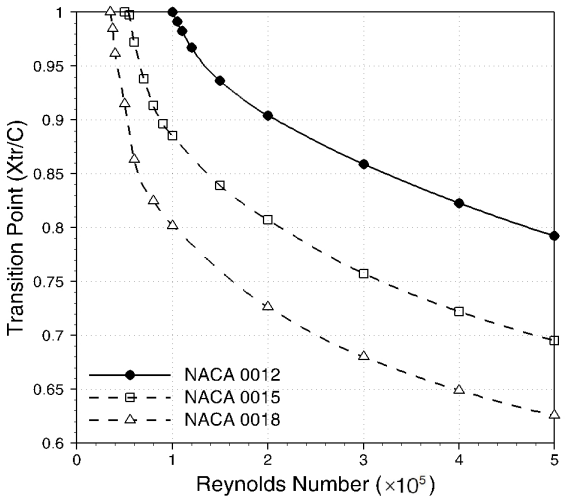

Figure 9. Variations of the transition point with the Reynolds number for the NACA 0012, NACA 0015, and NACA 0018 airfoil profiles at an angle of attack of zero degrees. The transition location over an airfoil is a strong function of the Reynolds number and moves toward the downstream as the Reynolds number decreases. The lower critical Reynolds number is defined as the velocity for which the transition point is located at the trailing edge of the airfoil.

equations were considered to describe the inviscid, irrotational flow outside the boundary layer and a two-equation integral formulation, i.e. integral momentum and kinetic energy shape parameter equations, was employed to represent the viscous boundary layer. The results of this study indicated that the transition location of an airfoil profile is strongly dependent on the Reynolds number and moves downstream (upstream) as the Reynolds number decreases (increases). The lower critical Reynolds number was then evaluated as a velocity at which the flow becomes laminar over the airfoil, which corresponds to the conditions that the transition point located at the trailing edge of the airfoil. The lower critical Reynolds number was consequently determined to be 1×10^5, 5×10^4, and 3.5×10^4 for the NACA 0012, NACA 0015, and NACA 0018 airfoils, respectively. The variations of the transition point with the angle of attack was further studied. It was observed that the transition point suddenly moves toward the leading edge with increasing the angle of attack.

Table 3. Variations of the transition location with the Reynolds number at an angle of attack of zero degrees for the NACA 0012 airfoil. The transition point moves downstream with decreasing the Reynolds number and finally locates at the trailing edge of the airfoil, i.e. $x_{tr}/c \cong 1$.

Reynolds Number	Lift Coefficient (C_L)	Drag Coefficient (C_D)	Transition Point (x_{tr}/c)
5.00×10^5	0.0	0.00617	0.7923
4.00×10^5	0.0	0.00668	0.8229
3.00×10^5	0.0	0.00768	0.8591
2.00×10^5	0.0	0.01020	0.9042
1.50×10^5	0.0	0.01299	0.9362
1.20×10^5	0.0	0.01540	0.9673
1.10×10^5	0.0	0.01624	0.9829
1.05×10^5	0.0	0.01660	0.9912
1.00×10^5	0.0	0.01694	1.0
0.90×10^5	0.0	0.01739	1.0
0.80×10^5	0.0	0.01796	1.0

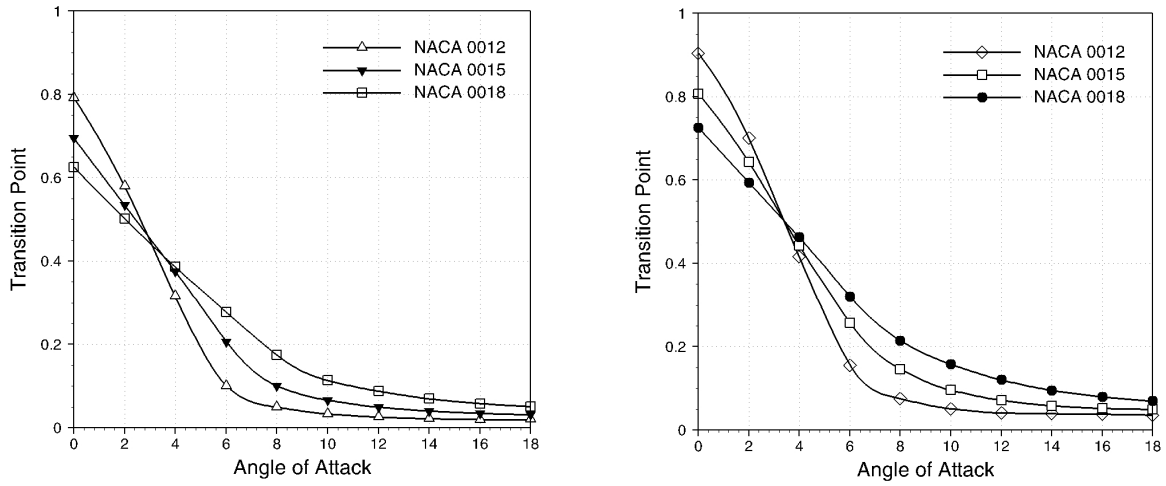

Figure 10. Variations of the transition point with the angle of attack over the NACA 0012, NACA 0015, and NACA 0018 airfoil profiles for the Reynolds numbers of (a) 5×10^5 and (b) 2×10^5.

References

[1]Mueller, T. J., Pohlen, L. J., Conigliaro, P. E., and Jansen, B. J. Jr., "The Influence of Free-Stream Disturbances on Low Reynolds Number Airfoil Experiments," *Experiments in Fluids*, Vol. 1, No. 1, 1983, pp. 3-14.

[2]Cengel, Y. A., and Cimbala, J. M., *Fluid Mechanics: Fundamentals and Applications*, 2nd ed., McGraw Hill, New York, 2010.

[3]Carmichael, B. H., "Low Reynolds Number Airfoil Survey," NASA Report No. 165803, 1981.

[4]Mueller, T. J., and Batill, S. M., "Experimental Studies of Separation on a Two-Dimensional Airfoil at Low Reynolds Numbers," *AIAA Journal*, Vol. 20, No. 4, 1982, pp. 457-463.

[5]Lissaman, P. B. S., "Low-Reynolds-Number Airfoils," *Annual Reviews of Fluid Mechanics*, Vol. 15, No. 1, 1983, pp. 223-239.

[6]Kraemer, K., "Airfoil Profiles in a Critical Reynolds Number Region," NASA Technical Translation, NASA-TT-F-14959, 1973.

[7]Mueller, T. J., "The Influence of Laminar Separation and Transition on Low Reynolds Number Airfoil Hysteresis," *Journal of Aircraft*, Vol. 22, No. 9, 1985, pp. 763-770.

[8]Brendel, M., and Mueller, T. J., "Boundary-Layer Measurements on an Airfoil at Low Reynolds Numbers," *Journal of Aircraft*, Vol. 25, No. 7, 1988, pp. 612-617.

[9]Johansen, J., and Sorensen, J. N., "Prediction of Laminar/Turbulent Transition in Airfoil Flows," *Journal of Aircraft*, Vol. 36, No. 4, 1999, pp. 731-734.

[10]Arnal, D., and Casalis, G., "Laminar-Turbulent Transition Prediction in Three-Dimensional Flows," *Progress in Aerospace Sciences*, Vol. 36, No. 2, 2000, pp. 173-191.

[11]Sousa, J. M. M., and Silva, L. M. G., "Transition Prediction in Infinite Swept Wings Using Navier-Stokes Computations and Linear Stability Theory," *Computers and Structures*, Vol. 82, No. 17-19, 2004, pp. 1551-1560.

[12]Lian, Y., and Shyy, W., "Laminar-Turbulent Transition of a Low Reynolds Number Rigid or Flexible Airfoil," *AIAA Journal*, Vol. 45, No. 7, 2007, pp. 1501-1513.

[13]Kurotaki, T., Sumi, T., and Atobe, T., "Numerical Simulation around Airfoil with Natural Transition in High Reynolds Numbers," *18th AIAA Computational Fluid Dynamics Conference*, AIAA 2007-3841, Miami, FL, 2007.

[14]Wang, L., Fu, S., Carnarius, A., Mockett, C., and Thiele, F., "A Modular RANS Approach for Modeling Laminar–Turbulent Transition in Turbomachinery Flows," *International Journal of Heat and Fluid Flow*, Vol. 34, No. 1, 2012, pp. 62-69.

[15]Hosseinverdi, S., and Fasel, H., "Direct Numerical Simulations of Transition to Turbulence in Two-Dimensional Laminar Separation Bubbles," *51st AIAA Aerospace Sciences Meeting*, AIAA 2013-0264, Grapevine, TX, 2013.

[16]Hatman, A., and Wang, T., "A Prediction Model for Separated Flow Transition," *Journal of Turbomachinery*, Vol. 121, No. 3, 1999, pp. 594-602.

[17]Volino, R. J., and Hultgren, L. S., "Measurements in Separated and Transitional Boundary Layers Under Low-Pressure Turbine Airfoil Conditions," *Journal of Turbomachinery*, Vol. 123, No. 2, 2001, pp. 189-197.

[18]Fitzgerald, E. J., and Mueller, T. J., "Measurements in a Separation Bubble on an Airfoil Using Laser Velocimetry," *AIAA Journal*, Vol. 28, No. 4, 1990, pp. 584-592.

[19]O'Meara, M. M., and Mueller, T. J., "Laminar Separation Bubble Characteristics on an Airfoil at Low Reynolds Numbers," *AIAA Journal*, Vol. 25, No. 8, 1987, pp. 1033-1041.

[20]Raffel, M., Favier, D., Berton, E., Rondot, C., Nsimba, M., and Geissler, M., "Micro-PIV and ELDV Wind Tunnel Investigations of the Laminar Separation Bubble Above a Helicopter Blade Tip," *Measurement Science and Technology*, Vol. 17, No. 7, 2006, pp. 1652-1658.

[21]Burgmann, A., Brücker, S., and Schröder, W., "Scanning PIV Measurements of a Laminar Separation Bubble," *Experiments in Fluids*, Vol. 41, No. 2, 2006, pp. 319-326.

[22]Yang, Z., and Hu, H., "Laminar Flow Separation and Transition on a Low-Reynolds-Number Airfoil," *Journal of Aircraft*, Vol. 45, No. 3, 2008, pp. 1067-1070.

[23]Drela, M., "XFOIL: An Analysis and Design System for Low Reynolds Number Airfoils," *Low Reynolds number aerodynamics*, 1989, pp. 1-12.

[24]Drela, M., and Giles, M. B., "Viscous-Inviscid Analysis of Transonic and Low Reynolds Number Airfoils," *AIAA Journal*, Vol. 25, No. 10, 1987, pp. 1347-1355.

[25]Shyy, W., Klevebring, F., Nilsson, M., Sloan, J., Carroll, B., and Fuentes, C., "Rigid and Flexible Low Reynolds Number Airfoils," *Journal of Aircraft*, Vol. 36, No. 3, 1999, pp. 523-529.

[26]Ramanujam, G., Özdemir, H., and Hoeijmakers, H. W. M., "Improving Airfoil Drag Prediction," *Journal of Aircraft*, Vol. 53, No. 6, 2016, pp. 1844-1852.

[27]Van Isngen, J., "The e^N Method for Transition Prediction. Historical Review of Work at TU Delft," *38th Fluid Dynamics Conference and Exhibit*, AIAA 2008-3830, Seattle, WA, 2008.

[28]Gleyzes, C., Cousteix, J., and Bonnet, J. L., "Theoretical and Experimental Study of Low Reynolds Number Transitional Separation Bubbles," *Conference on Low Reynolds Number Airfoil Aerodynamics*, UNDAS-CP-77B123, Notre Dame, IN, 1985, pp. 137-152.

[29]Sahu, R., and Patnaik, B. S. V., "CFD Simulation of Momentum Injection Control Past a Streamlined Body," *International Journal of Numerical Methods for Heat and Fluid Flow*, Vol. 21, No. 8, 2011, pp. 980-1001.

[30]Miller, D., "Lift, Drag and Moment of a NACA 0015 Airfoil," Department of Aerospace Engineering, OHIO State University, 2008.

[31]Nakano, T., Fujisawa, N., Oguma, Y., Takagi, Y., and Lee, S., "Experimental Study on Flow and Noise Characteristics of NACA0018 Airfoil," *Journal of Wind Engineering and Industrial Aerodynamics*, Vol. 95, No. 7, 2007, pp. 511-531.

[32]Gregory, N., and O'Reilly, C. L., "Low-Speed Aerodynamic Characteristics of NACA0012 Airfoil Section, Including the Effects of Upper-Surface Roughness Simulating Hoar Frost," Aeronautical Research Council, R&M No. 3726, 1970.

[33]Bæk, P., and Fuglsang, P., "Experimental Detection of Transition on Wind Turbine Airfoils," *Proceedings of European Wind Energy Conference*, Marseille, France, 2009.

[34]Timmer, W. A., "Two-Dimensional Low-Reynolds Number Wind Tunnel Results for Airfoil NACA 0018," *Wind Engineering*, Vol. 32, No. 6, 2008, pp. 525-537.
[35]Rooij, R. V., "Modification of the Boundary Layer Calculation in RFOIL for Improved Airfoil Stall Prediction," Delft University of Technology, Report IW-96087R, Netherlands, 1996.
[36]Ma, D., Zhao, Y., Qiao, Y., and Li, G., "Effects of Relative Thickness on Aerodynamic Characteristics of Airfoil at a Low Reynolds Number," *Chinese Journal of Aeronautics*, Vol. 28, No. 4, 2015, pp. 1003-1015.
[37]Timmer, W. A., and Van Rooij, R. P. J. O. M., "Summary of the Delft University Wind Turbine Dedicated Airfoils," *Journal of Solar Energy Engineering*, Vol. 125, No. 4, 2003, pp. 488-496.
[38]Yousefi, K., Saleh, R., and Zahedi, P., "Numerical Study of Blowing and Suction Slot Geometry Optimization on NACA 0012 Airfoil," *Journal of Mechanical Science and Technology*, Vol. 28, No. 4, 2014, pp. 1297-1310.
[39]Yousefi, K., and Saleh, R., "Three-Dimensional Suction Flow Control and Suction Jet Length Optimization of NACA 0012 Wing," *Meccanica*, Vol. 50, No. 6, 2015, pp. 1481-1494.
[40]Galbraith, M. C., and Visbal, M. R., "Implicit Large Eddy Simulation of Low-Reynolds-Number Transitional Flow past the SD7003 Airfoil," *40th Fluid Dynamics Conference and Exhibit*, AIAA 2010-4737, Chicago, IL, 2010.